Article:

Li, H.-Y., Liu, Y. and Zhu, Z.Q. orcid.org/0000-0001-7175-3307 (2018) Comparative study of air-gap field modulation in flux reversal and Vernier permanent magnet machines. IEEE Transactions on Magnetics, 54 (11). 8105206. ISSN 0018-9464

https://doi.org/10.1109/TMAG.2018.2837898

Comparative Study of Airgap Field Modulation in Flux Reversal and Vernier Permanent Magnet Machines

H .Y. Li, *Student Member, IEEE,* Y. Liu, and Z. Q. Zhu, *Fellow, IEEE*

Department of Electronic and Electrical Engineering, University of Sheffield, Sheffield, S1 3JD, U. K.

In this paper, the torque production mechanisms of flux reversal permanent magnet (FRPM) machine and Vernier PM machine are analyzed and compared based on airgap field modulation. Working harmonics of PM magnetomotive force (MMF) and airgap permeance in two machines are analytically identified and compared, indicating that the fundamental PM MMF together with all permeance harmonics contribute to the torque production of Vernier machine whereas all PM MMF harmonics but only fundamental permeance in FRPM machine produces the torque. Thanks to the utilized large DC component of airgap permeance, the torque density of Vernier machine is revealed to be better. Influence of critical parameters on machine performance, such as PM thickness and slot width ratio of the modulation pole, is also investigated. It shows that FRPM machine is more sensitive to the design parameters. Both finite element analysis (FEA) and experimental validation are conducted to verify the conclusions.

***Index Terms*—Field modulation, flux reversal, permanent magnet, Vernier machine.**

I. INTRODUCTION

With the recently developed theories of airgap field modulation [1-3], the working principles of many machine topologies, such as magnetically geared machine [4-6], stator permanent magnet (PM) machines [7] [8], Vernier machine [9], variable flux reluctance machine [10] etc., have been analyzed and/or re-recognized now.

Among various airgap field modulation-based machines, FRPM and Vernier machines are two typical topologies offering advantage of simple mechanical structure, such as single airgap, surface-mounted PM (SPM) structure and integrated modulation iron poles, as shown in Fig. 1. For both machines, the PM magnetomotive force (MMF) harmonics (resulted from SPM) interact with the permeance harmonics produced by modulation iron poles, thus producing abundant field harmonics in the airgap. The pole pair number of the main harmonic of the PM field is no longer required to be equal to that of the armature field [8] [11], which differs from the conventional PM machine.

Up to now, most papers are focused on topology evolution or performance improvement of either FRPM [12-15] or Vernier machine [16-19], and the differences of airgap field modulation and corresponding performance comparison between two machines have never been addressed, thus will be the main focus of this paper.

II. MACHINE CONFIGURATION AND WORKING PRINCIPLE

The operation principles of FRPM and Vernier machines are firstly deduced from the perspective of generator, and the no-load back-EMF is used to assess and compare their performance. For simplicity, some assumptions are made as: 1) the saturation of the stator and rotor core is neglected; 2) the end-effect and fringing effect of the machine are neglected; 3) the PMs are radially-magnetized.

Manuscript received ** **, 2018; revised ** **, 2018; accepted ** **, 2018. Date of publication ** **, 2018; date of current version ** **, 2018. Corresponding author: Z. Q. Zhu (e-mail: z.q.zhu@sheffield.ac.uk).

By using simple MMF-permeance model [15, 19], the no-load airgap flux density of the machines can be given as

$$B(\theta,t)=F_{PM}(\theta,t)\Lambda(\theta,t) \quad (1)$$

where F_{PM} (θ,t) is the PM MMF produced by the SPM structure, and Λ (θ,t) is the air-gap permeance produced by the salient modulation iron poles.

A. FRPM Machine

As shown in Fig. 1(a), for a conventional FRPM machine, the PMs are mounted on the inner surface of stator teeth with identical polarities of two adjacent PMs belong to different stator teeth, and the rotor consists of several iron poles, producing static PM MMF and rotating permeance harmonics.

The static PM MMF can be expressed in Fourier series, as

$$F_{PM}(\theta)=\sum_{i=1,2,3\cdots}^{\infty}F_i\sin(i\frac{N_s}{2}\theta) \quad (2)$$

where N_s is the number of stator slot, i is the order of Fourier series, F_i is the corresponding Fourier coefficient and is [15]

$$F_i=\frac{2F}{i\pi}\left[1-\cos(i\frac{\pi}{2}k)+\cos(i\frac{\pi}{2}(2-k))-\cos(i\pi)\right] \quad (3)$$

where k=(1-w_{so}/τ_s), $\tau_s=2\pi/N_s$, F is related to the remanence (B_r), height (h_m), and relative permeability (μ_r) of the PM material, and $F=B_rh_m/\mu_r\mu_0$.

Regarding the permeance distribution, it can be written as

$$\Lambda(\theta,t)=\sum_{q=0,1,2\cdots}^{\infty}\Lambda_q\cos\left[qN_r(\theta-\theta_0-\Omega_rt)\right] \quad (4)$$

where Ω_r is the angular speed of the rotor, N_r is the rotor pole number, q is the order of Fourier series, and Λ_q is the corresponding Fourier coefficient, which is [20]

$$\Lambda_0=\frac{\mu_0}{g'}(1-1.6\beta\frac{w}{\tau}) \quad (5)$$

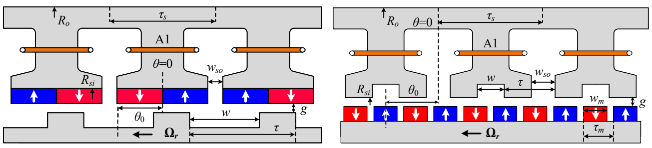

(a) (b)

Fig. 1. Schematics of machines with single airgap, SPM structure and integrated modulation iron poles. (a) FRPM machine. (b) Vernier machine.

TABLE I
WORKING HARMONICS OF PM MMF AND PERMEANCE DISTRIBUTION

	FRPM	Vernier
PM MMF (F_i)	F_i (i=1, 2, 3…)	F_1
Permeance (Λ_q)	Λ_1	Λ_q (q=0, 1, 2…)
Back-EMF (E_a)	$n_c l R_{si}\Omega_r\cdot\Lambda_1\sum_{i=1,2,3\cdots}^{\infty} w^f{}_i F_i$	$n_c l R_{si}\Omega_r\cdot F_1\sum_{q=0,1,2\cdots}^{\infty} w^v{}_q \Lambda_q$
Weight factor (w)	$w^f{}_i=\frac{\pm N_r}{iN_s/2\pm N_r}\cdot \sin\left[(iN_s/2\pm N_r)\pi/N_s\right]$	$w^v{}_q=\frac{1}{2}\frac{p_m}{p_m\pm q2N_s}\cdot\sqrt{(2-2\cos(p_m 2\pi/N_s))}$

TABLE II
PARAMETERS OF FRPM AND VERNIER MACHINES (UNITS: MM)

	Analytical		FEA		Prototype	
Parameters	FRPM	Vernier	FRPM	Vernier	FRPM	Vernier
Stator slot number N_s	12	6	12	6	12	6
Rotor pole number N_r,p_m			10			
Outer radius R_o			45			
Axial length l			25			
Airgap length g			0.5			
PM property B_r, μ_r			1.2T, 1.05			
Stator inner radius R_{si}	30		30.2	28.4	29.3	21
PM thickness h_m	2		1.2	2.4	2	2.5
Slot width ratio w/τ	0.6		0.65	0.5	0.7	0.5
Stator slot opening w_{so}	2		1.5	7.4	2.5	5.6

$$g'=g+h_m/\mu_r \tag{6}$$

$$\Lambda_q=-\beta\frac{4}{\pi q}\frac{\mu_0}{g'}\left[\frac{1}{2}+\frac{(qw/\tau)^2}{0.78125-2(qw/\tau)^2}\right]\sin(1.6\pi q\frac{w}{\tau}) \tag{7}$$

$$\beta=\frac{1}{2}\left[1-1/\sqrt{1+(w/2g')^2}\right] \tag{8}$$

Substituting (1) with (2)-(8), the flux density is rewritten as

$$B(\theta,t)=\frac{1}{2}\sum_{i=1,2,3\cdots}^{\infty}\sum_{q=0,1,2\cdots}^{\infty}F_i\Lambda_q\sin\left[\left(\frac{iN_s}{2}\pm qN_r\right)\theta\mp qN_r\left(\theta_0+\Omega_r t\right)\right] \tag{9}$$

Considering the flux through the single coil A1, it is

$$\lambda_A(t)=n_c\int B(\theta,t)ds=n_c lR_{si}\int_{-\pi/N_s}^{\pi/N_s}B(\theta,t)d\theta$$
$$=\sum_{i=1,2,3\cdots}^{\infty}\sum_{q=0,1,2\cdots}^{\infty}\frac{F_i\Lambda_q n_c lR_{si}}{iN_s/2\pm qN_r}\sin\left[\left(\frac{iN_s}{2}\pm qN_r\right)\frac{\pi}{N_s}\right]\sin\left[\mp qN_r\left(\theta_0+\Omega_r t\right)\right] \tag{10}$$

where n_c is the number of turns per coil, l is the machine stack length, R_{si} is the stator inner radius.

Correspondingly, its back-EMF can be obtained as

$$e_A(t)=-d\lambda_A(t)/dt=$$
$$\sum_{i=1,2,3\cdots}^{\infty}\sum_{q=1,2,3\cdots}^{\infty}\frac{\pm qN_rF_i\Lambda_q n_c lR_{si}\Omega_r}{iN_s/2\pm qN_r}\sin\left[\left(\frac{iN_s}{2}\pm qN_r\right)\frac{\pi}{N_s}\right]\cos\left[qN_r\left(\theta_0+\Omega_r t\right)\right] \tag{11}$$

From (9) and (11), it is clear that abundant harmonics exist in the no-load airgap flux density, however, only those with same q can contribute to the back-EMF with same frequency.

B. Vernier Machine

As shown in Fig. 1(b), the rotor of Vernier machine is of SPM structure and the modulation iron poles are located on the stator, resulting in static permeance and rotating PM MMF harmonics. Theoretically, the number, width and depth of the auxiliary slots on the stator tooth are changeable, making the permeance distribution more complex. In this study, each tooth has one auxiliary slot and its width is set as equal to the stator slot opening (w=w_{so}) while its depth is regarded as infinite for simplicity. Thus, the number of modulation pole is $2N_s$, and the expressions of (5)-(8) are still feasible [19]. The static permeance distribution is then expressed as

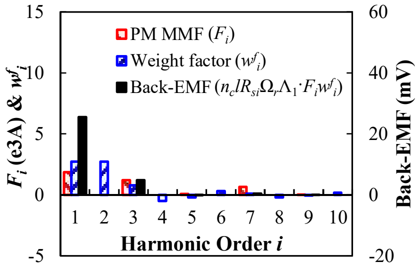

Fig. 2. Harmonics of PM MMF of FRPM machine and their weight factors and contributions to back-EMF (n_c=1, n=400r/min).

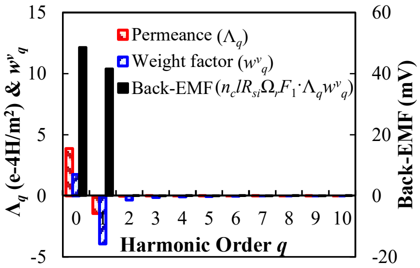

Fig. 3. Harmonics of permeance distribution of Vernier machine and their weight factors and contributions to back-EMF (n_c=1, n=400r/min).

TABLE III
MAIN COMPONENTS CONTRIBUTING TO THE BACK-EMF

	Back-EMF	Principal component	Secondary component
FRPM	30.6mV	Λ_1 with $w^f{}_1F_1$ (83.6%)	Λ_1 with $w^f{}_3F_3$ (15.5%)
Vernier	90.2mV	F_1 with $w^v{}_0\Lambda_0$ (53.9%)	F_1 with $w^v{}_1\Lambda_1$ (46.0%)

$$\Lambda(\theta)=\sum_{q=0,1,2\cdots}^{\infty}\Lambda_q\cos\left(2qN_s\theta\right) \tag{12}$$

The rotating PM MMF of Vernier machine can be written as

$$F_{PM}(\theta,t)=\sum_{i=1,2,3\cdots}^{\infty}F_i\sin\left[ip_m(\theta-\theta_0-\Omega_r t)\right] \tag{13}$$

$$F_i=\frac{4F}{i\pi}\left[\sin(i\pi/2)\sin(i\pi\alpha/2)\right] \tag{14}$$

where p_m is the pole-pair number of rotor PM, and α=w_m/τ_m.

Substituting (1) with (12)-(14), the flux density is

$$B(\theta,t)=\frac{1}{2}\sum_{i=1,2,3\cdots}^{\infty}\sum_{q=0,1,2\cdots}^{\infty}F_i\Lambda_q\sin\left[\left(ip_m\pm q2N_s\right)\theta-ip_m\left(\theta_0+\Omega_r t\right)\right] \tag{15}$$

Similarly, the flux and back-EMF of coil A1 are deduced as

$$\lambda_A(t)=n_c\int B(\theta,t)ds=n_c lR_{si}\int_0^{2\pi/N_s}B(\theta,t)d\theta=$$
$$\frac{1}{2}\sum_{i=1,2,3\cdots}^{\infty}\sum_{q=0,1,2\cdots}^{\infty}\frac{n_c lR_{si}F_i\Lambda_q}{ip_m\pm q2N_s}\sqrt{(2-2\cos(\frac{ip_m}{N_s}2\pi))}\cos\left[ip_m\left(\theta_0+\Omega_r t\right)+\theta_1\right] \tag{16}$$

$$e_A(t)=-d\lambda_A(t)/dt=$$
$$\frac{1}{2}\sum_{i=1,2,3\cdots}^{\infty}\sum_{q=0,1,2\cdots}^{\infty}\frac{ip_m\Omega_r n_c lR_{si}F_i\Lambda_q}{ip_m\pm q2N_s}\sqrt{(2-2\cos(\frac{ip_m}{N_s}2\pi))}\sin\left[ip_m\left(\theta_0+\Omega_r t\right)+\theta_1\right] \tag{17}$$

Again, abundant no-load flux density harmonics exist in Vernier machines. However, only those with same i contribute to the back-EMF with same frequency, as seen from (17).

C. Different Working Harmonics of Two Machines

Comparing (11) and (17), it is found that the working harmonics of PM MMF and permeance distribution are different between two machines, as summarized in TABLE I. For FRPM machine, all PM MMF harmonics (F_i) but only fundamental permeance (Λ_1) contributes to the production of back-EMF, and there is a unique weight factor (w^f_i) for each harmonic of PM MMF. In contrast, for Vernier machine, only fundamental PM MMF (F_1) but all permeance harmonics (Λ_q)

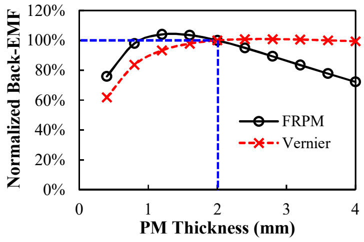

Fig. 4. Influence of PM thickness h_m on back-EMF.

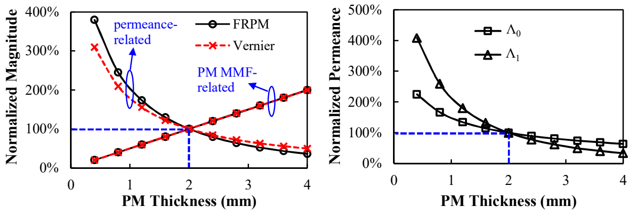

(a) (b)

Fig. 5. Influence of h_m. (a) On permeance and PM-MMF. (b) On Λ_0 and Λ_1.

are effective. Similarly, there has a weight factor ($w^v{}_q$) for each permeance harmonic.

To compare the performance between FRPM and Vernier machines and also quantify the contribution of each harmonic, the back-EMFs of two machines with same rotor pole number (N_r=p_m=10) are analytically calculated, with their basic parameters listed in TABLE II.

For the FRPM machine, Fig. 2 shows the magnitude (F_i), weight factor ($w^f{}_i$) and back-EMF contribution of each PM MMF harmonic. As can be seen, only odd harmonics of PM MMF exist and $w^f{}_i$ rapidly decreases with i. Therefore, two main components contribute to the back-EMF and F_1 accounts for absolute proportion (83.6%), see TABLE III.

For the Vernier machine, Fig. 3 shows the magnitude (Λ_q), weight factor ($w^v{}_q$) and back-EMF contribution of each permeance harmonic. In addition to Λ_1, the large Λ_0 is utilized to interact with F_1, producing additional back-EMF component with even higher proportion (53.9%), see TABLE III.

Although F_1 and Λ_1 interact to produce back-EMF for both two machines, it is clear that Vernier machines always have better performance than FRPM machines. This can be explained by the fact that for FRPM machines, additional back-EMF component resulted from F_3 is minor due to the low weight factor $w^f{}_3$; for Vernier machines, additional back-EMF component resulted from Λ_0 is considerable, thanks to its large magnitude.

III. Influence of Critical Parameters

Based on the parameters in TABLE II, the superior performance of Vernier machine has been revealed. Further, it is essential to analyze the influence of critical parameters on machine performance.

A. Influence of PM Thickness

Since PM thickness h_m directly affects the magnitude of PM MMF and equivalent airgap length, its influence on machine performance is obvious, Fig. 4. The performance of original h_m=2mm is set as benchmark, so as to provide a clear illustration. As can be seen, there is an optimal h_m for both machines. For the FRPM machine, the optimal h_m is smaller and then the back-EMF rapidly decreases with h_m. In contrast,

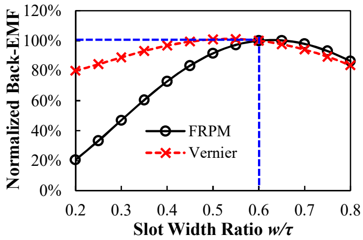

Fig. 6. Influence of slot width ratio w/τ on back-EMF.

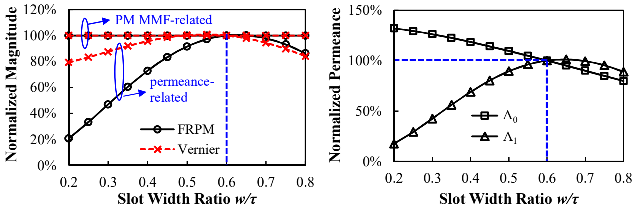

Fig. 7. Influence of w/τ. (a) On permeance and PM-MMF. (b) On Λ_0 and Λ_1.

for the Vernier machine, the back-EMF only slightly decreases when h_m is too large. Based on TABLE III, the influence of h_m on either permeance-related (for FRPM, it is Λ_1; for Vernier, it is $w^v{}_0\Lambda_0$+$w^v{}_1\Lambda_1$) or PM MMF-related (for FRPM, it is $w^f{}_1F_1$+$w^f{}_3F_3$; for Vernier, it is F_1) component of the back-EMF is separated, Fig. 5 (a). It shows that the influence of h_m on permeance-related component of two machines is different, due to the different variation trends of Λ_0 and Λ_1 against h_m, Fig. 6 (b). Since the back-EMF of FRPM machine only depends on Λ_1 which is more sensitive to h_m, h_m cannot be selected too large, resulting in small PM MMF and inferior performance.

B. Influence of Slot Width Ratio

Fig. 6 shows the influence of slot width ratio of modulation iron poles (w/τ) on machine performance, and w/τ=0.6 is set as benchmark to normalize the influence. As can be seen, the performance of FRPM machine is more sensitive to w/τ. Again, this can be further explained by the influence of w/τ on permeance-related and PM MMF-related component of the back-EMF since Λ_1 is more sensitive to w/τ, Fig. 7.

IV. Performance Comparison by FEA

To validate the previous analysis, both FRPM and Vernier machines are globally optimized in FEA, aiming at maximum torque under the same copper loss of 20W. Their parameters are listed in TABLE II. Fig. 8 shows the cross-section and flux distribution of the two machines, while Fig. 9 compares their torque performance. As can be seen, within the whole copper loss range, the Vernier machine always has higher torque density, and its rated torque is 2.9Nm which is 93% higher than the FRPM machine (1.5Nm). Fig. 10 (a) compares the power factors of two machines. As can be seen, the power factors decrease with the load condition (copper loss) and the Vernier machine has higher power factor, thanks to the higher PM flux linkage [21]. Under the same copper loss of 20W, Fig. 10 (b) compares the efficiency of the two machines. Again, it shows that the Vernier machine has better efficiency due to the improved torque. The influence of h_m and w/τ on average torque is shown and compared in Fig. 11. As can be seen, the optimal h_m of the FRPM machine is only 1.2mm,

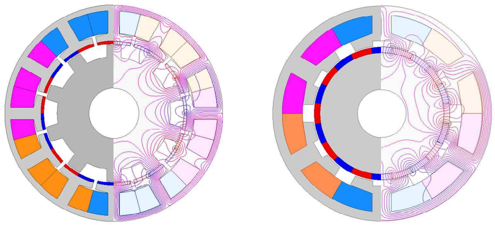

(a) (b)

Fig. 8. Flux distribution of the two machines. (a) FRPM. (b) Vernier.

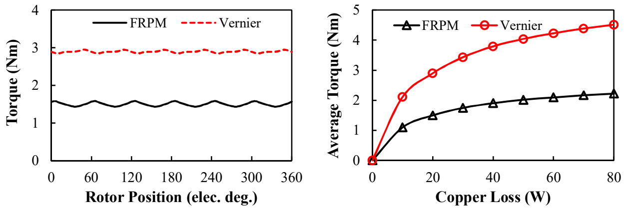

(a) (b)

Fig. 9. Torque performance. (a) Waveform. (b)Variation against copper loss.

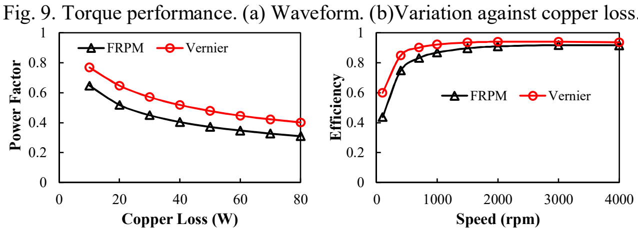

(a) (b)

Fig. 10. Machine performance. (a) Power factor. (b)Efficiency.

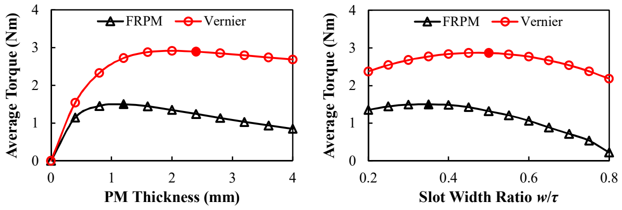

(a) (b)

Fig. 11. Influence of parameters on average torque. (a) h_m. (b) w/τ.

while that of the Vernier machine is 2.4mm. In addition, the torque of the FRPM machine is more sensitive to both h_m and w/τ, which is consistent with Fig. 4 and Fig. 6.

V. Experimental Validation

Except for analytical and FE analyses, both FRPM prototype and Vernier prototypes are manufactured and tested. Fig.12 shows the machine structures, and TABLE I lists their parameters. It should be noted that the parameters of the prototypes are not strictly identical to the optimal FEA models when considering some practical manufacturing issues.

Fig. 13 shows the measured, analytical, and FE-predicted back-EMFs of the two machines at n=400rpm. Under the same slot filling factor, the number of series turns per phase is 84 for the FRPM machine, and it is 100 for the Vernier machine. As can be seen, the measured back-EMF matches well with the analytical and FEA results, and the Vernier machine has 86% higher measured fundamental back-EMF than the FRPM machine.

By suppling three-phase windings with fixed dc current (I_a=-2I_b=-2I_c=I_{dc}=0.6I_{rated}, and the rated current I_{rated} is corresponded to p_{cu}=20W), the variation of static torque can

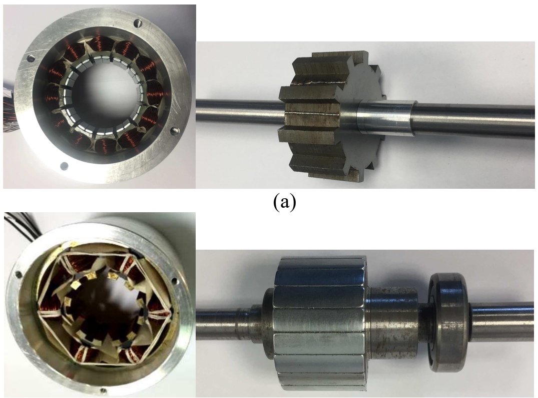

(a)

(b)

Fig. 12. Prototypes. (a) FRPM (N_s=12, N_r=10). (b) Vernier (N_s=6, p_m=10).

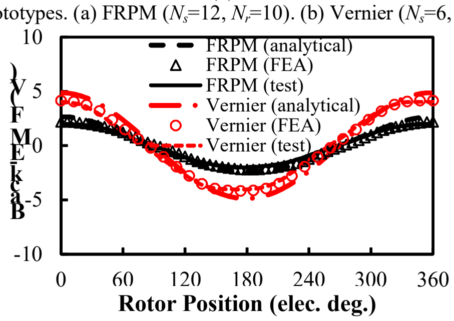

Fig. 13. Measured, analytical, and FE-predicted back-EMFs. (n=400rpm)

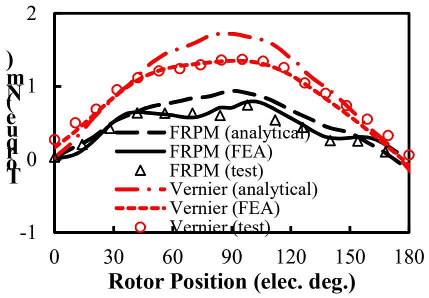

Fig. 14. Measured, analytical, and FE-predicted static torques. (I_a=-2I_b=-2I_c)

be measured [22], as shown in Fig. 14. As can be seen, good agreements between the FEA results and test results can be observed while the analytical results are larger due to the assumptions (neglect of saturation, infinite slot depth etc.) in analytical derivations. More importantly, the maximum measured torque of the Vernier machine is 1.35Nm, which is 80% larger than that of the FRPM machine. Therefore, the higher torque density of the Vernier machine over the FRPM machine is verified.

VI. Conclusion

In this paper, FRPM machine and Vernier machine have been analyzed and compared based on the unified theory of airgap field modulation. It has been found that Vernier machine is more likely to have higher torque density than FRPM machine, thanks to the utilized large DC component of airgap permeance. In addition, the performance of FRPM machine is shown to be more sensitive to the design parameters, i.e. PM thickness and slot width ratio. All the findings have been validated by both FEA and experiment.

REFERENCES

[1] K. Atallah, and D. Howe, "A novel high-performance magnetic gear," *IEEE Trans. Magn.*, vol.37, no.4, pp.2844-2846, 2001.

[2] M. Cheng, P. Han, and W. Hua, "A general airgap field modulation theory for electrical machines," *IEEE Trans. Ind. Electron.*, vol. 64, no. 8, pp. 6063–6074, 2017.

[3] Z. Q. Zhu and Yue Liu, "Analysis of air-gap field modulation and magnetic gearing effect in fractional slot concentrated winding permanent magnet synchronous machines," *IEEE Trans. Ind. Electron.*, vol. 65, no. 5, pp. 3688–3698, 2018.

[4] K. T. Chau, Z. Dong, J. Z. Jiang, L. Chunhua, and Z. Yuejin, "Design of a magnetic-geared outer-rotor permanent-magnet brushless motor for electric vehicles," *IEEE Trans. Magn.*, vol. 43, no. 6, pp. 2504-2506, 2007.

[5] K. Atallah, J. Rens, S. Mezani, and D. Howe, "A novel 'pseudo' direct-drive brushless permanent magnet machine," *IEEE Trans. Magn.*, vol. 44, no. 12, pp. 4605-4617, 2008.

[6] L. L. Wang, J. X. Shen, P. C. K. Luk, W. Z. Fei, C. F. Wang, and H. Hao, "Development of a magnetic-geared permanent-magnet brushless motor," *IEEE Trans. Magn.*, vol. 45, no. 10, pp. 4578–4581, Sep. 2009.

[7] Z. Z. Wu and Z. Q. Zhu, "Analysis of air-gap field modulation and magnetic gearing effects in switched flux permanent magnet machines," *IEEE Trans. Magn.*, vol. 51, no. 5, p. 8105012, 2015.

[8] D. S. More and B. G. Fernandes, "Analysis of flux-reversal machine based on fictitious electrical gear," *IEEE Trans. Energy Convers.*, vol. 25, no. 4, pp. 940–947, Dec. 2010.

[9] R. Qu, D. Li, and J. Wang, "Relationship between magnetic gears and Vernier machines," in *Electr. Mach. Syst. (ICEMS 2011), IEEE Int. Conf.*, Aug. 2011.

[10] L. R. Huang, J. H. Feng, S. Y. Guo, J. X. Shi, W. Q. Chu, and Z. Q. Zhu, "Analysis of torque production in variable flux reluctance machine," *IEEE Trans. Energy Convers.*, vol. 32, no. 4, pp. 1297–1308, 2017.

[11] A. Toba and T. A. Lipo, "Generic torque-maximizing design methodology of surface permanent-magnet vernier machine," *IEEE Trans. Ind. Appl.*, vol. 36, no. 6, pp. 1539–1546, 2000.

[12] R. Deodhar, S. Andersson, I. Boldea, and T. J. E. Miller, "The flux reversal machine: A new brushless doubly-salient permanent magnet machine," *IEEE Trans. Ind. Appl.*, vol. 33, no. 4, pp. 925–934, Jul. 1997.

[13] C. Wang, S. A. Nasar, and I. Boldea, "Three-phase flux reversal machine (FRM)," *Proc. Inst. Elect. Eng.—Electr. Power Appl.*, vol. 146, no. 2, pp. 139–146, Mar. 1999.

[14] I. Boldea, J. Zhang, and S. A. Nasar, "Theoretical characterization of flux reversal machine in low speed servo drives-the pole-PM configuration," *IEEE Trans. Ind. Appl.*, vol. 38, no. 6, pp. 1549–1557, Dec. 2002.

[15] Y. Gao, R. Qu, D. Li, J. Li, and L. Wu, "Design of three-phase flux-reversal machines with fractional-slot windings," *IEEE Trans. Ind. Appl.*, vol. 52, no. 4, pp. 2856–2864, July 2016.

[16] S. Niu, S. L. Ho, W. N. Fu, and L. L. Wang, "Quantitative comparison of novel Vernier permanent magnet machines," *IEEE Trans. Magn.*, vol. 46, no. 6, pp. 2032–2035, 2010.

[17] S. L. Ho, S. Niu, and W. N. Fu, "Design and comparison of Vernier permanent magnet machines," *IEEE Trans. Magn.*, vol. 47, no. 10, pp. 3280–3283, 2011.

[18] D. Li, R. Qu, and Z. Zhu, "Comparison of Halbach and dual-side Vernier permanent magnet machines," *IEEE Trans. Magn.*, vol. 50, no. 2, pp. 10–13, Feb. 2014.

[19] D. Li, R. Qu, and J. Li, "Analysis of torque capability and quality in Vernier permanent-magnet machines," *IEEE Trans. Ind. Appl.*, vol. 52, no. 1, pp. 125–135, 2016.

[20] Z. Q. Zhu and D. Howe, "Instantaneous magnetic field distribution in brushless permanent magnet dc motors, part III: Effect of stator slotting," *IEEE Trans. Magn.*, vol. 29, no. 1, pp. 143–151, Jan. 1993.

[21] D. Li, R. Qu, and T. A. Lipo, "High power factor Vernier permanent magnet machines," *IEEE Trans. Ind. Appl.*, vol. 50, no. 6, pp. 3664–3674, 2014.

[22] Z. Q. Zhu, "A simple method for measuring cogging torque in permanent magnet machines," in *Proc. IEEE Power Energy Soc. Gen. Meet.*, 2009, pp. 1–4.